Ultra-Fast Finite Element Analysis of Brushless PM Machines Based on Space-Time Transformations

Dan M. Ionel
A. O. Smith Corp.
12100 W. Park Place
Milwaukee, WI 53224-9512
Email:dionel@aosmith.com

Mircea Popescu
Motor Design Ltd.
4 Scotland Street
Ellesmere SY12 0EG, UK
Email: mircea.popescu@motor-design.com

Abstract—A computationally-efficient method is proposed for the steady-state performance simulation of brushless permanent magnet (BLPM) motors. Only a minimum number of magneto-static FEA solutions are used in conjunction with space-time transformations, which are based on the periodicity specific to synchronous machines. For an example interior permanent magnet (IPM) motor with six teeth per pole, a single magneto-static FE solution was employed to estimate the flux density time waveforms in the stator teeth and yoke. Other results include core losses, back emf and torque. The extension of the method to fractional slot topologies with reduced number of teeth is discussed with reference to a 9-slot 6-pole IPM motor example. The results compare satisfactorily with those obtained from substantially more laborious time-stepping FEA.

Index Terms – Brushless (BL) permanent-magnet (PM) motor, AC synchronous machine, IPM motor drive, finite-element analysis (FEA), flux density waveform, back emf, core loss.

I. INTRODUCTION

Finite Element Analysis (FEA) of the electromagnetic field is well established as a mathematical tool for improving the accuracy of electric machine simulations. Despite the well recognized advantages of considering exact geometry details and the non-linearity of steel, the penetration of FEA is still relatively low in the early stages of the industrial design process and in the optimization studies that involve the analysis of hundreds or thousands of candidate designs. For these tasks, more popular are methods based on rather simplified geometries and improvements of the traditional analytical formulations, such as those described by Hendershot and Miller [1].

Until relatively recently, both the pre-processing, which involves object description inclusive of the geometry and meshing, as well as the processing, i.e. solving the large systems of equations, were limiting factors to wider FEA acceptance and implementation. Over the years, the challenge of finding the right balance between computational speed and precision was addressed, for example, by methods based on non-linear equivalent magnetic circuits, such as the one proposed by Lovelace *et al.* [2].

However, based on recent developments that allow the close integration of parametric geometric modeling and drafting (CAD/CAE) software, fully automatic meshing capabilities, product and material databases etc, the amount of time required for a simulation remains the only real barrier for practical applications. Ideally, a detailed simulation of a motor and drive system should be based on a coupled field and circuit model, as, for example, the one proposed by Mohammed *et al.* [3]. Nevertheless, for many motor engineering problems simplified FEA may be acceptable provided that significant reduction is achieved in terms of computational resources.

For DC machines (with brushes), Demerdash *et al.* described detailed, as well as simplified methods, for computing the back emf and the inductances [4]. For induction motors, Williamson *et al.* developed frequency domain models that include only one rotor slot pitch and one stator phase belt [5]. In this manner, the computational effort was substantially reduced because the smallest possible region was employed and the time variation of fundamental quantities was accounted through a single FE solution in complex numbers.

The concepts from the present paper, which are introduced with application to brushless (BL) permanent magnet (PM) motors, can be extended on a more general basis to electronically controlled synchronous machines. Unlike typical FEA that employs hundreds of time-steps to solve the electromagnetic diffusion equation, the new method only uses a minimum number of magneto-static FE solutions of the Poisson equation in conjunction with space-time transformations that exploit the repetitive features of motor geometry and the periodicity of the electromagnetic field.

For some machine topologies, as little as a single magneto-static solution maybe required. In the studied examples, a significant reduction in computational time was achieved while maintaining satisfactory precision for performance estimation. The steady-state analysis is performed in the abc reference frame, therefore avoiding the known pitfalls of dq theory.

II. ELECTROMAGNETIC FIELD ANALYSIS

The revolving magnetic field produced in the air-gap of a BLPM machine by a rotor, which moves with the angular electric speed ω, can be expressed by a Fourier series

$$B_m(t,\theta) = \sum_{\nu=1}^{\infty} B_{m\nu} \sin\left(\nu\omega t + \nu p\theta\right) \tag{1}$$

as a function of time t and space angular coordinate θ, where p is the number of pole pairs.
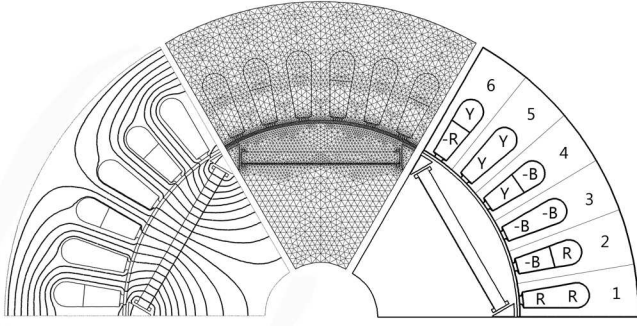
Fig. 1. Finite Element (FE) model for one pole of an IPM motor with a distributed winding. Only one open-circuit magneto-static field solution is employed for the space-time transformations of Figs. 2–3.

Sinusoidal currents flowing in a 3-phase stator winding produce in the air-gap an armature reaction revolving field

$$B_a(t,\theta) = \sum_{\nu=1}^{\infty} B_{a\nu} \times$$

$$\sum_{f,b} \sum_{m=1}^{3} \cos\left[\omega t \pm \nu p\theta + \gamma_0 \pm (\nu \mp 1)(m-1)\frac{2\pi}{3}\right] \quad (2)$$

where the plus sign corresponds to the forward f moving waves, the minus to the backward b moving waves and γ_0 is the torque angle. In a balanced system, the resultant electric fundamental is a forward moving wave. The amplitude of the armature reaction waves

$$B_{a\nu} = \frac{3}{\pi}\mu_0 \frac{wk_{o\nu}k_{w\nu}}{k_s k_c g_0 \nu p} I_{pk} \quad (3)$$

is proportional with the total number of series turns per phase w, the harmonic factors for slot opening $k_{o\nu}$ and winding $k_{w\nu}$ and the peak value of the phase current I_{pk}. The amplitude is inversely proportional with the saturation factor k_s, the Carter factor k_C and the air-gap length g_0.

The previous equations are valid for the normal component of flux density and do not include the slotting harmonics. An additional simplification is introduced by neglecting the higher order harmonics ($\nu > 1$) of the armature reaction and considering only its fundamental wave ($\nu = 1$). The basis and the implications of this assumption are further discussed in another section. It should be noted that the harmonics of the open-circuit field established by the PM rotor are still included in the model. Based on (1) and (2), in this case the expression of the air-gap field

$$B_g(t,\theta) = \sum_{\nu=1}^{\infty} [B_{m\nu} \sin(\nu\omega t + \nu p\theta)] +$$

$$B_{a1}\cos(\omega t + p\theta + \gamma_0) \quad (4)$$

as a function of time t at given angular coordinate θ is of the same form with the expression of the function of θ at given t, provided that the two variables are linked by the space-time linear transformation

$$p\theta = \omega t. \quad (5)$$
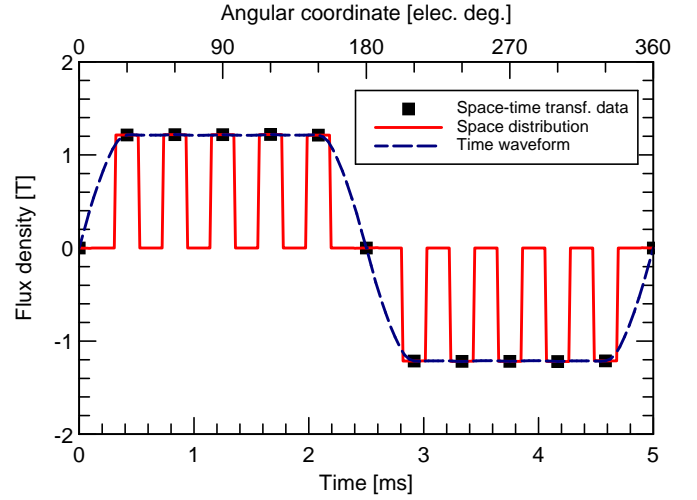
Fig. 2. Flux density in the center of the teeth for the motor of Fig. 1 operating in open-circuit at 4,000rpm.

At steady-state, by further considering the magnetic flux law together with the observation that in a typical electrical machine the flux density in the teeth has a substantially radial component B_r and in the yoke (back iron) a substantially tangential component B_t, the field in the stator core will satisfy the periodicity condition

$$B_{r,t}(t,r,\theta) = B_{r,t}\left(t + \frac{pk\theta_s}{\omega}, r, \theta + k\theta_s\right) \quad (6)$$

where θ_s is the slot pitch measured in elec. deg. and k is a positive integer.

For the rather small components of the tangential flux density in the teeth and of the radial flux density in the yoke, equation (6) is somewhat intuitively acceptable, under the previously introduced assumptions. For induction motor stators it was shown through a detailed study based on numerical analysis in the frequency domain that the complex magnetic vector potential A satisfies a periodicity condition on the edges of a the phase-belt region [5]. Taking into account that

$$B_r = \frac{\partial A}{r\partial\theta} , \qquad B_t = -\frac{\partial A}{\partial r} \quad (7)$$

the condition translates in periodicity for the flux density components.

Based on the above rationale, the time function of the magnetic field at any given point (r,θ) in the stator can be "constructed" (estimated) based on the values of the field at a given time t at points of the same r and integral increments of the slot pitch, i.e. $(r, \theta + k\theta_s)$. The procedure is explained with reference to the example of Fig.1, in which the finite element mesh in the stator has the same configuration for every slot pitch. However, repetitive meshing is not an absolute requirement, provided that space mapping/interpolation techniques are employed.

For the magneto-static solution of Fig.1, the spatial distribution of the field along a radius that passes through the middle of the teeth is shown in Fig. 2. The FEA was performed
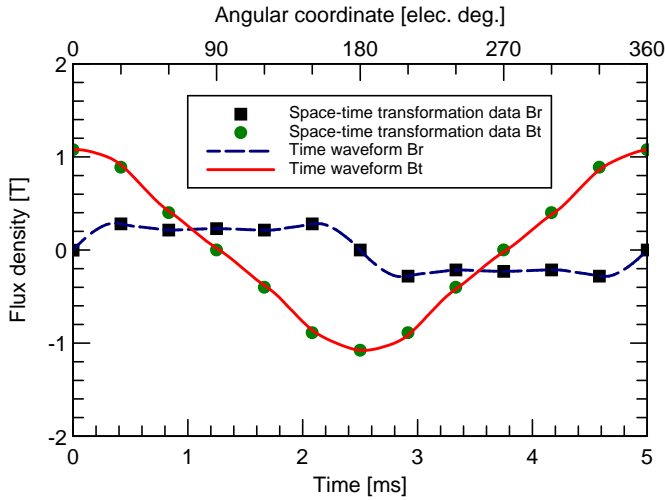
Fig. 3. Flux density in a mid-yoke point centrally located above the 6th slot in the motor of Fig. 1 operating in open-circuit at 4,000rpm.

only on the smallest required domain of one pole (180 elec. deg). Also shown is the time waveform for the radial flux density in the center of the last tooth positioned within the slot pitch number 6. This data was obtained from 360 time-stepped solutions with a counter-clockwise (CCW) moving rotor. As a general rule, if not specified otherwise, the angular coordinate starts in the reference point – in this case the center of the last tooth – and extends in the direction opposite to the rotor movement.

Over half period, seven equidistant points of the time waveform can be actually estimated based on the space-time transformation using the values of the flux density in the center of the five full teeth and two half teeth, which are included in the computational domain. By employing the anti-periodicity condition, a total of thirteen points are calculated over one full period. The discrete flux density waveforms derived in this manner can then be used for Fourier analysis. In the example considered, based on a single magneto-static solution, harmonics can be calculated up to and inclusive of the fifth electrical order.

The same algorithm can be applied for any point within the 6th slot pitch. Figure 3 illustrates the good agreement between the time waveform of the flux density in the point positioned in the radial center of yoke above the last tooth and the corresponding space distribution from the magneto-static solution of Fig.1. In the yoke not only the tangential but also the radial flux density can be significant. In this case, depending on the particular motor geometry and field pattern, there maybe points exhibiting differences between the space and time results.

The procedure is valid both for open-circuit and load simulations (Figs. 4–6). The flux plot of Fig. 4 illustrates through the pattern of flux lines, together with the colors of the flux density plots, the substantially radial component of the field in the teeth and the substantially radial component in the yoke.
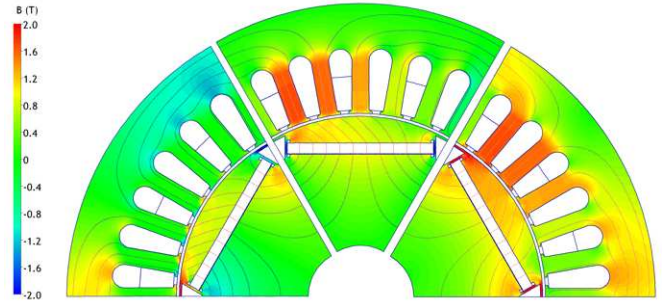
Fig. 4. Rated load flux lines and color plots of (CCW from right to left): modulus, radial and tangential flux density, respectively. The field is substantially radial in the teeth and substantially tangential in the yoke.
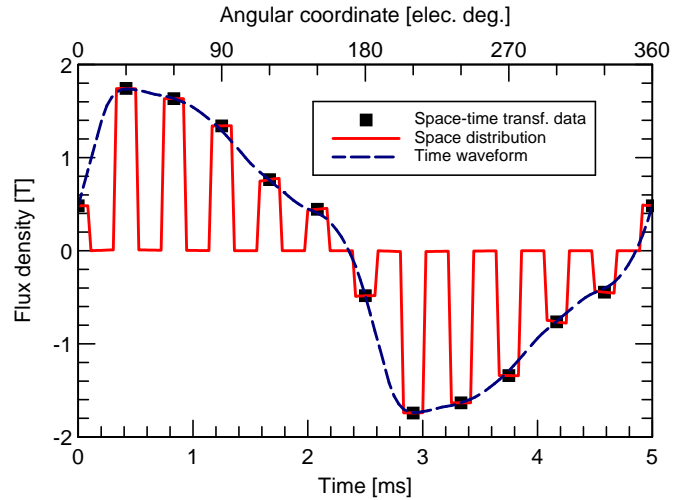
Fig. 5. On-load flux density in the center of the teeth. The data for the space-time transformation is provided by the single magneto-static FE solution shown in Fig. 4.

III. MACHINE PERFORMANCE ESTIMATION

A. Core Losses

The harmonics of the waveforms calculated with the previously described procedure can be employed for the estimation of stator core losses. For each harmonic, the peak value of the flux density in any finite element is computed from the radial and tangential components

$$B_\nu = \sqrt{B_{r\nu}^2 + B_{t\nu}^2} \qquad (8)$$

The eddy current specific losses per unit of mass are given by the equation

$$w_e = \sum_{\nu=1}^{\nu_{max}} k_{e\nu} \left(\nu f_1, B_\nu \right) \cdot \left(\nu f_1 \right)^2 \cdot B_\nu^2 \qquad (9)$$

and the hysteresis specific losses by

$$w_h = \sum_{\nu=1}^{\nu_{max}} k_{h\nu} \left(\nu f_1, B_\nu \right) \cdot \left(\nu f_1 \right) \cdot B_\nu^2 . \qquad (10)$$

The variation of the core loss coefficients with frequency and peak resultant flux density was demonstrated in [6]. The
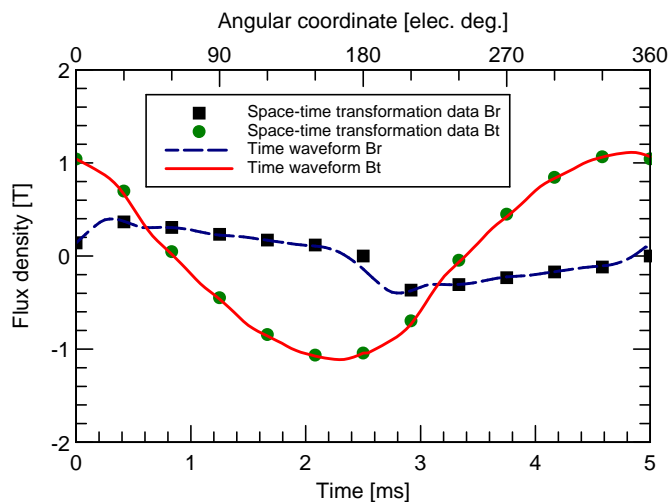
Fig. 6. Flux density in a mid-yoke point centrally located above the 6th slot in the load example of Fig. 4. Both the tangential and the radial field components are plotted.
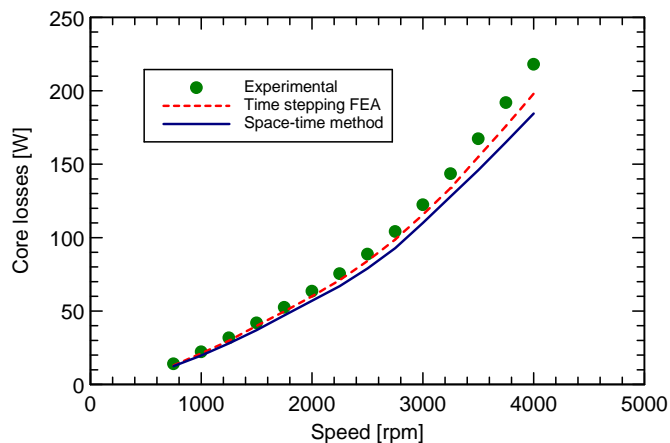
Fig. 7. Open-circuit core losses for the example motor of Figs. 1–3.

Fourier harmonic analysis implies the superposition principle under the assumption that the main contribution is due to the fundamental frequency f_1.

The method was validated on a case study for the open-circuit operation of the 184-frame 3-phase 6-pole IPM motor prototype that served as an example for Figs. 1–6. The computational results of Fig. 7 are systematically lower than the test data, which is in line with expectations being given that the effect of manufacturing, such as punching the laminations, shrink fitting the core in the frame etc, is not included in the mathematical model. Between the time stepping and the harmonic simulation, the underestimation increases from a maximum of approximately 10% to about 15%. Factors contributing to the lower values calculated with (8)–(10) include the limited number of harmonics and the absence of a correction factor for the minor hysteresis loops.

Rotor position	Virtual position of phase coils Slot number					
[elec. deg.]	1	2	3	4	5	6
0	R	R	-B	-B	Y	Y
30	R	-B	-B	Y	Y	-R
60	-B	-B	Y	Y	-R	-R
90	-B	Y	Y	-R	-R	B
120	Y	Y	-R	-R	B	B
150	Y	-R	-R	B	B	-Y
180	-R	-R	B	B	-Y	-Y

B. Back EMF

The tooth waveforms can also be used for the computation of the flux linkage through virtual stator coils wound around each tooth and of the per-phase back emf based, for example, on the procedure presented in [1]. In the following, another approach, which is inspired by Eastham [7], will be described for calculating the back emf based on the magnetic vector potential in the slots.

The procedure is introduced with reference to Table I. For the simplicity of explanation, a single layer fully pitched winding is employed instead of the double layer short-pitched arrangement depicted in Fig.1. However, the concept can be extended to any type of winding pattern. Only one magneto-static FEA is performed with the rotor positioned under the stator core as shown in Fig.1. This θ_0 position is identified in Table I as the 0 deg. position.

The flux linkage per unit of length through one turn of a coil can be calculated as the difference between the average values of the magnetic vector potential A in the two slots where the coil sides are placed, respectively. For example, for the yellow (Y) phase a fully pitched coil placed in slot 6 returns in slot 12, which is not part of the FEA region. Taking into account the per-pole anti-periodicity, the flux linkage through this coil is equal to:

$$\Phi_{y,6-12}(\theta_0) = w_c \left(A_6 - A_{12} \right) \ell_{Fe} = 2A_6 w_c \ell_{Fe} \qquad (11)$$

where w_c is the number of turns in the coil and ℓ_{Fe} is the effective stator core length. A similar calculation can be made for the coil of the yellow phase that spans from slot 5 to 11. The result is then added to the one from (11) in order to determine the flux linkage through the entire phase winding.

Instead of moving the rotor in the CCW direction and performing additional FEA, the coils are virtually shifted by one slot in the opposite direction as shown in Table I. From the calculation point of view, this is equivalent to a rotor movement of exactly 30 elec. deg. For this second position in the sequence, the flux linkage in the yellow phase is calculated based on the average magnetic vector potential from slots 4 and 5. The procedure continues in one-slot increments until a half electric cycle is covered.

Figure 8 includes magnetic vector potential A waveforms and further illustrates the virtual coil shift concept. The discrete points that can be employed for a space-time transfor-
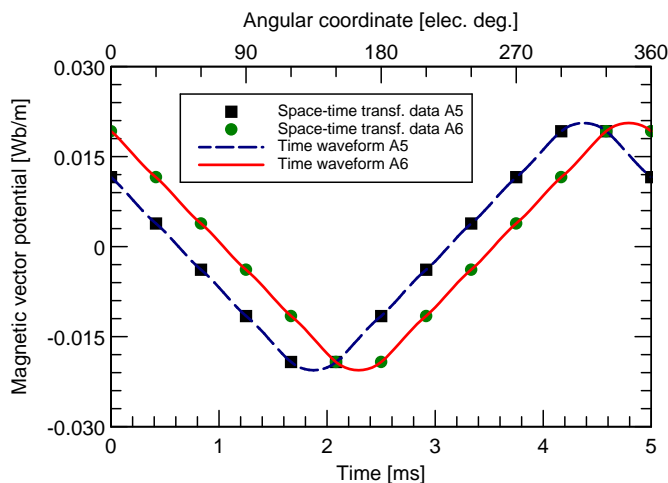
Fig. 8. Waveforms of average magnetic vector potential in the 5th and 6th slot and the space-time transformation data obtained with the virtual coil shifting method of Table I.
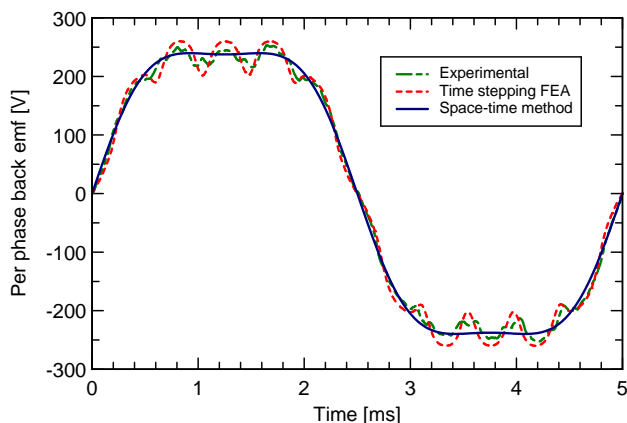
Fig. 9. Open-circuit back emf for the example IPM motor of Figs. 1-3.

mation for the coil side placed in slot number 6 are provided by the average values of A in the slots in the exact sequence 6, 5, 4, 3, 2, 1. For the coil side from the slot number 5 the exact sequence of 5, 4, 3, 2, 1 is complemented at the end by the value of A from slot 6 taken with changed sign, due to the anti-periodicity between adjacent poles. In Fig. 8, for the clarity of the plot, the origin of the angular coordinate was selected to be different for each spatial distribution and to correspond to the placement of the coil side in the magneto-static FEA (see the first line of Table 1).

The space-time transformation procedure can be employed for any winding pattern, including the one shown in Fig. 1. In the recommended procedure, in order to avoid the differentiation errors, the back emf harmonics are individually calculated from the flux linkage harmonics and then contributions added to estimate the waveform. For the prototype IPM motor, satisfactory agreement was achieved between measurements, time-stepping FEA and the simplified space-time calculations, which do not include the effect of the higher-order slotting harmonics (Fig. 9).
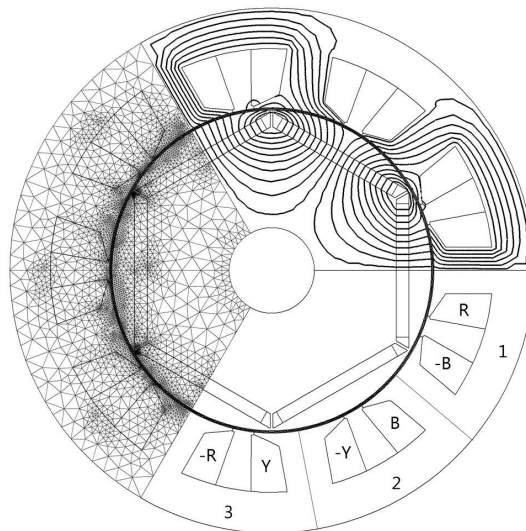
Fig. 10. FE model for a 6-pole 9-slot IPM motor with concentrated coils wound around each tooth. One pole pair is considered for simulating open-circuit operation.
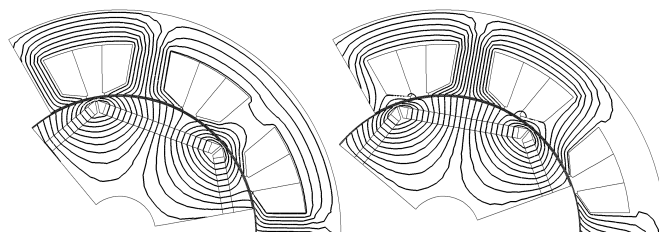
Fig. 11. Two additional FE solutions with the rotor positioned at 10 and 20 mech. deg. are employed for the space-time transformations of Figs. 12–13.

C. Average Torque

The method previously described can be used in conjunction with other techniques for computing the electromagnetic torque with minimal computational effort. The Maxwell stress harmonic method introduced in [8], employs only magneto-static field solution in order to compute the average torque of a brushless PM motor operated from an ideally sine-wave current regulated drive.

IV. EXTENSION OF THE METHOD

The new method based on space-time transformations takes full advantage of the repetitive geometry of stator cores with identical slot pitches. For some machine topologies there simply may not be enough teeth to ensure satisfactory computation based on a single magneto-static FE solution. In this case, multiple solutions corresponding to different rotor positions and load current distributions are employed following careful planning in order to minimize the computational effort.

The design example of Figs.10-15 has the widely-used configuration with three slots for each pole pair and concentrated coils around each tooth. In this case, for the center tooth position only four points for a space-time transformation can
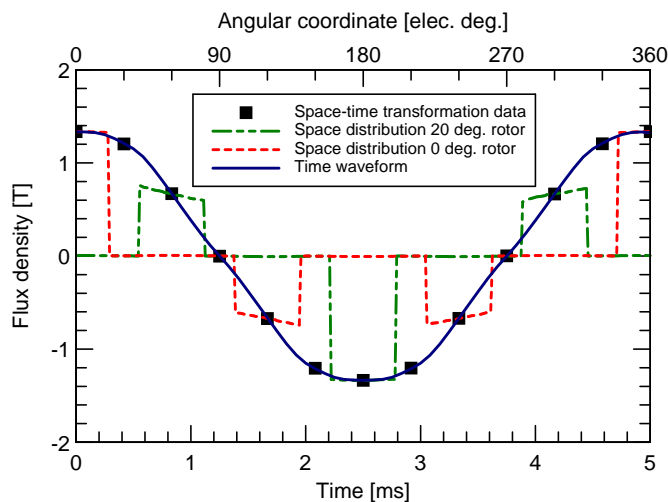
Fig. 12. Flux density in the center of the teeth for the 9-slot 6-pole IPM motor example operating in open-circuit at 4,000rpm.
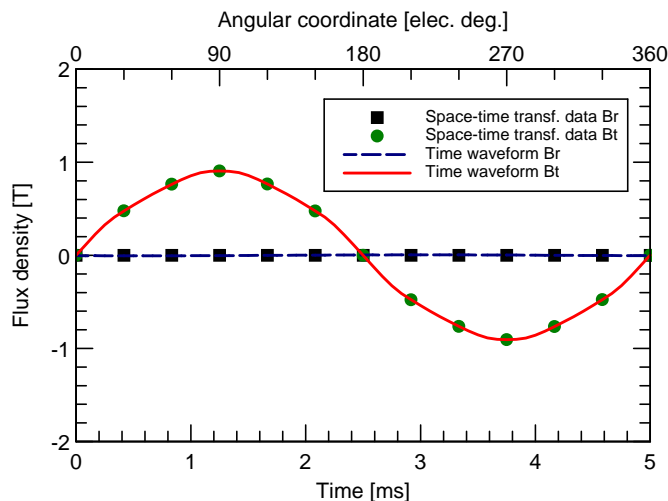
Fig. 13. Flux density in the yoke (centrally above slot) for the 9-slot 6-pole IPM motor example operating in open-circuit at 4,000rpm.

be derived from the magneto-static solution of Fig. 10. From such information only the fundamental wave can be computed.

At open-circuit operation, a minimum of two additional simulations – with the rotor positioned at 10 and 20 mech. deg., respectively (Fig. 11) – are required in order to estimate up to inclusively the fifth electrical harmonic. The graph of Fig. 12 includes the spatial distribution of the radial component of flux density along a surface that passes through the middle of the stator teeth. For the clarity of the plot, the field distributions are shown only for the 0 and 20 deg. rotor position. The angular coordinate is in the rotor reference frame, measured CW from the left edge of the flux plot of Figs. 10-11.

In terms of points to be used for a space-time transformation on the graph of Fig. 12, the initial rotor position provides the points located at 0, 120, 240 and 360 elec. deg. The 10 deg. rotor position supplies the points for 30, 150 and 270 elec.
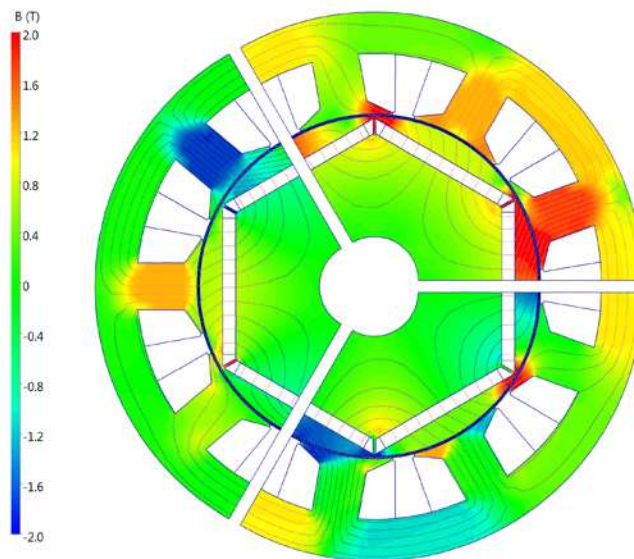
Fig. 14. Rated load flux lines and color plots of: modulus, radial and tangential flux density, respectively (CCW from right to left). The field is substantially radial in the teeth and substantially tangential in the yoke.

deg. The 20 deg. rotor position yields the values at 60, 180 and 300 elec. deg. Finally the remainder of the points shown are calculated based on the previous data, using the center-pole symmetry condition specific to open-circuit field distribution. For example, the value of flux density for 330 elec. deg. is equal to the one for 30 elec. deg. A similar procedure is employed for the back iron, where for the design example the flux density is substantially tangential (Fig. 13).

For load operation, when there is no field symmetry within a pole, one magneto-static FE in the initial position of Fig. 14 plus three other solutions of different rotor position and current distribution are in principle required in order to equidistantly cover one electrical cycle. The first solution provides four data points to be used for space-time transformation, while the other three solutions supply three points each.

The graph of Fig. 15 further illustrates the space-time relationship for the example motor operating on-load. The radial flux density in each tooth is identical in shape and the waveforms of adjacent teeth are separated in space by 120 elec. deg. For the on-load tangential flux density waveform in the back iron, it is interesting to note that the peak value is only marginally higher than at open-circuit, while the top of the curve is flat indicating the presence of higher order harmonics.

V. DISCUSSION OF ASSUMPTIONS AND RESULTS

In principle, the procedures described in the previous sections can be implemented using the programming or scripting capabilities of commercially available electromagnetic FEA software. The space-time transformations examples from this paper were produced using the PC-FEA software [9].

The results of the new method show, within the scope of an analysis limited to relatively low order harmonics,
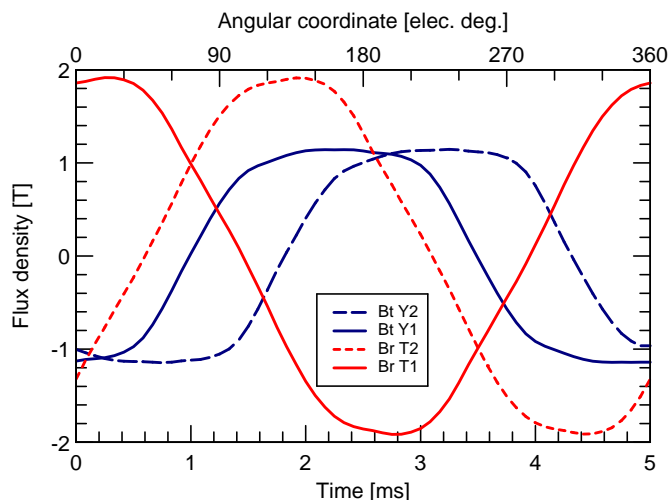
Fig. 15. Flux density in the center of two adjacent teeth and in the yoke (centrally above slot) for the rated operation of the IPM motor of Fig. 14.

Harmonic	Winding type			
factor	Distributed – 36 slots		Concentrated – 9 slots	
	Fully pitched	Short (5/6) pitched	Double layer	Double layer with skew
k_{w1}	0.966	0.933	0.866	0.827
k_{w3}	0.707	0.500	0.000	0.000
k_{w5}	0.259	0.067	0.866	0.165
k_{w7}	0.259	0.067	0.866	-0.118
k_{w9}	0.707	0.500	0.000	0.000
k_{w11}	0.966	0.933	0.866	-0.075
k_{w13}	0.966	0.933	0.866	0.064
k_{w15}	0.707	0.500	0.000	0.000
k_{w17}	0.259	0.067	0.866	0.049
k_{w19}	0.259	0.067	0.866	-0.044

Fig. 16. Variation of the slot opening factor for the IPM motor examples.

satisfactory agreement with more elaborate and substantially more resource consuming time-stepping FE computations. For open-circuit operation this is well in line with expectations, being given that the main assumption involved in this case, namely that the field is radial in the teeth and tangential in the yoke, is typically valid in practical machine designs of regular proportions. Furthermore, the yoke, which may contain both radial and tangential flux components, is generally a lower contributor in terms of both mmf drop and core losses in the overall performance of a typical BLPM motor.

For the simulation of load operation, the new method involves a more restrictive assumption, in that for the armature reaction mmf only the fundamental is considered and the other harmonics are neglected. Yet, in the magneto-static FEA that supplies the data for the space-time transformation, the actual stator winding pattern and currents are considered, instead of an ideal sine-wave distribution. In principle, this may lead to errors that should be carefully investigated for each particular type of machine design. However, state of the art brushless PM motors for sine-wave current regulated controllers are purposely designed for low harmonic content and hence may naturally fit to a satisfactory degree the assumptions of the new method.

The example IPM of Fig.1 employs a 5/6 short-pitched two-layer lap winding that greatly reduces the fifth and the seventh stator mmf harmonics due to the very low values of the corresponding winding factors (Table 2). Even if for the other examples the harmonic winding factors may be relatively higher, it should be kept in mind that the armature flux density harmonics are also reduced by other elements, including the harmonic order itself, as reflected in (3). The armature harmonics are inversely proportional with the air-gap length. Hence they are expected to be less significant in surface mounted PM motors – which typically have a larger equivalent air-gap – than in IPM motors, such as those studied in the paper.

The slot opening factor [10],

$$k_{o\nu} = \frac{2}{\nu\beta_0} \sin \frac{\nu\beta_0}{2} , \qquad (12)$$

which is neglected in the conventional theory maybe particularly effective in fractional slot designs. The integral 36-slot 6-pole IPM motor example has a relatively small slot opening β_0 with a value of 7.5 elec. deg. On the other hand, the 9-slot 6-pole IPM motor with concentrated windings of Fig. 10 has a typical large opening of 22.5 elec. deg., which has a relatively high impact even on the lower order harmonics as illustrated in Fig. 16. As a separate note, for this motor configuration a stator to rotor relative axial skew of half-slot drastically reduces the effect of fifth and seventh harmonics on global parameters, such as back emf and torque ripple.

In terms of flux density harmonics, the waveform in the tooth of the concentrated winding IPM motor operating at rated-load (Fig. 15) includes a fifth and a seventh order of approximately 2.5% and 2% of the fundamental, respectively, while the third harmonic is practically negligible. On the other hand, in the yoke, under the same operating conditions, the third saturation harmonic is substantial at 14.5% of the fundamental, while the fifth is very small at 2% and the seventh is practically zero.

The previous discussion provides hints on other possible

applications of the new space-time transformation method. For example, the FE based technique could be employed only to calculate the fundamental and possibly the third order harmonic. In this case, the benefits would include the minimization of the number of magneto-static FE solutions and the filtering of the high-order mmf harmonics. The effect of the higher order mmf and of the slotting (permeanace, zig-zag) harmonics could be separately estimated, especially for the tooth tip regions, through analytical means and added to the FE space-time transformation results.

VI. Conclusion

The proposed method fills in a much needed gap in the simulation tools available for brushless PM motor drives and is of particular interest to initial machine sizing and optimization, when computational speed is of the essence. Satisfactory motor performance estimation is achieved with only a very small number of magneto-static FE solutions and space-time transformations specific to electrical machines.

For an IPM motor with a distributed winding and six teeth per pole, a single magneto-static FE solution was employed in order to calculate up to the fifth electric order the harmonics of the steady-state magnetic field in the stator core. For another IPM example with a concentrated around-the-tooth winding and three teeth per pole pair, a minimum of three magneto-static FE solutions were used to obtain similar style results. In both cases, as well as for other anticipated design configurations of practical interest, the computational time is reduced by one or, possibly, two orders of magnitude as compared with typical time-stepping FEA. The new method includes the estimation of core losses and back emf and can be effectively combined with procedures for minimum-effort computation of electromagnetic torque.

References

[1] J. R. Hendershot and T. J. E. Miller, *Design of Brushless Permanent-Magnet Motors*. Mentor, OH and Oxford, UK: Magna Physics and Oxford University Press, 1994.

[2] E. C. Lovelace, T. M. Jahns, and J. Lang, "A saturating lumped-parameter model for an interior pm synchronous machine," *IEEE Trans. on IAS*, vol. 38, no. 3, pp. 645–650, May/June 2002.

[3] O. A. Mohammed, S. Liu, and Z. Liu, "Physical modeling of pm synchronous motors for integrated coupling with machine drives," *IEEE Trans. on MAG*, vol. 41, no. 5, pp. 1628–1631, May 2005.

[4] N. Demerdash, T. Nehl, F. A. Fouad, and A. Arkadan, "Analysis of the magnetic field in rotating armature electronically commutated dc machines by finite elements," *IEEE Trans. on PAS*, vol. PAS-103, no. 7, pp. 1829–1836, July 1984.

[5] S. Williamson, L. Lim, and M. Robinson, "Finite-element models for cage induction motor analysis," *IEEE Trans. on IAS*, vol. 26, no. 6, pp. 1007–1017, Nov/Dec 1990.

[6] D. M. Ionel, M. Popescu, M. I. McGilp, T. J. E. Miller, S. J. Dellinger, and R. J. Heideman, "Computation of core losses in electrical machines using improved models for laminated steel," *IEEE Trans. on IAS*, vol. 43, no. 6, pp. 1554–1564, Nov/Dec 2007.

[7] J. F. Eastham, *FEA of Electrical Machines – Private Communication*, University of Bath, Bath, UK, 1994.

[8] D. M. Ionel, M. Popescu, M. I. McGilp, T. J. E. Miller, and S. J. Dellinger, "Assessment of torque components in brushless permanent-magnet machines through numerical analysis of the electromagnetic field," *IEEE Trans. on IAS*, vol. 41, no. 5, pp. 1149–1158, Sept/Oct 2005.

[9] M. Olaru, M. I. McGilp, and T. J. E. Miller, *PC-FEA 5.5.2.1 for Windows – Software*, SPEED Laboratory, University of Glasgow, Glasgow, UK, 2008.

[10] D. M. Ionel, M. V. Cistelecan, T. J. E. Miller, and M. I. McGilp, "A new analytical method for the computation of air-gap reactances in 3-phase induction motors," in *IEEE IAS Conference, 1998*, vol. 1, Oct 1998, pp. 65–72.